Proc. Natl. Acad. Sci. USA
Vol. 95, pp. 4607–4612, April 1998
Medical Sciences

Regulation of transport pathways in tumor vessels: Role of tumor type and microenvironment

SUSAN K. HOBBS*†‡, WAYNE L. MONSKY*‡§, FAN YUAN*¶, W. GREGORY ROBERTS‖, LINDA GRIFFITH†, VLADIMIR P. TORCHILIN**, AND RAKESH K. JAIN*††

*Edwin L. Steele Laboratory, Department of Radiation Oncology, Massachusetts General Hospital and Harvard Medical School, 100 Blossom St., Cox-7, Boston, MA 02114; †Department of Chemical Engineering, Massachusetts Institute of Technology, 66-466, 25 Ames St., Cambridge, MA 02139; ‖Cellular and Molecular Medicine, Room 210, University of California at San Diego, 9500 Gilman Drive, La Jolla, CA 92093-0651; **Center for Imaging and Pharmaceutical Research, Massachusetts General Hospital and Harvard Medical School, Charlestown, MA 02138; and §Department of Radiological Sciences, Beth Israel–Deaconess Medical Center, 330 Brookline Avenue, Boston, MA 02215

Edited by Robert Langer, Massachusetts Institute of Technology, Cambridge, MA, and approved February 9, 1998 (received for review December 12, 1997)

ABSTRACT **Novel anti-neoplastic agents such as gene targeting vectors and encapsulated carriers are quite large (approximately 100–300 nm in diameter). An understanding of the functional size and physiological regulation of transvascular pathways is necessary to optimize delivery of these agents. Here we analyze the functional limits of transvascular transport and its modulation by the microenvironment. One human and five murine tumors including mammary and colorectal carcinomas, hepatoma, glioma, and sarcoma were implanted in the dorsal skin-fold chamber or cranial window, and the pore cutoff size, a functional measure of transvascular gap size, was determined. The microenvironment was modulated: (*i*) spatially, by growing tumors in subcutaneous or cranial locations and (*ii*) temporally, by inducing vascular regression in hormone-dependent tumors. Tumors grown subcutaneously exhibited a characteristic pore cutoff size ranging from 200 nm to 1.2 μm. This pore cutoff size was reduced in tumors grown in the cranium or in regressing tumors after hormone withdrawal. Vessels induced in basic fibroblast growth factor-containing gels had a pore cutoff size of 200 nm. Albumin permeability was independent of pore cutoff size. These results have three major implications for the delivery of therapeutic agents: (*i*) delivery may be less efficient in cranial tumors than in subcutaneous tumors, (*ii*) delivery may be reduced during tumor regression induced by hormonal ablation, and (*iii*) permeability to a molecule is independent of pore cutoff size as long as the diameter of the molecule is much less than the pore diameter.**

The hyperpermeability of tumor microvessels to large molecules has been observed in numerous studies, and it has been speculated that large therapeutic agents could be selectively delivered to the tumor (1–3). However, the upper limit of the size of the therapeutic agent that can traverse vessels of different tumors and how this is regulated is not well understood. We have recently measured the pore cutoff size of a human colon carcinoma, LS174T, grown subcutaneously in immunodeficient mice and found it to be between 400 and 600 nm (4). Furthermore, we have shown that vascular permeability of this colon carcinoma to albumin ($\approx$7 nm) is higher when grown in the liver than when grown subcutaneously (5). On the other hand, the vascular permeability of a human glioma, HGL21, was significantly reduced in the cranial microenvironment compared with the subcutaneous microenvironment (4). A similar decrease in the permeability to albumin was observed in the colon carcinoma grown subcutaneously when treated with anti-vascular endothelial growth factor (VEGF) antibody (6). These three separate observations lead to the following important questions. (*i*) Do all tumors grown in a given site have the same pore cutoff size or is it tumor-dependent? (*ii*) Is the pore cutoff size lower in the cranial than in the subcutaneous microenvironment? (*iii*) Is the pore cutoff size fixed or does it vary during tumor growth and regression? Despite their obvious importance to the design of therapeutic strategies, these questions have not been answered to date.

We report here that tumors that are grown in the subcutaneous microenvironment have a tumor-dependent functional pore cutoff size ranging from 200 nm to 1.2 μm, which is dramatically reduced when the tumor is grown in the cranial microenvironment. Furthermore, testosterone withdrawal results in a reduction of the pore cutoff size from 200 nm to less than 7 nm within 48 hr, in a testosterone-dependent tumor. The effective permeability to smaller macromolecules such as albumin is shown to be independent of the pore cutoff size. Basic fibroblast growth factor (bFGF)-induced vessels have a pore cutoff size similar to tumors, 200 nm. Macromolecular transport across blood vessels has been shown to occur via open gaps (interendothelial junctions and transendothelial channels), caveolae, vesicular vacuolar organelles (VVO), fenestrations, and phagocytosis (7–10). Using electron microscopy we show that the transport of nanoparticles occurs via open gaps. These studies suggest that tumors in the cranial microenvironment as well as tumors treated with hormone ablation therapies may have reduced transvascular transport of large macromolecules or nanoparticles used as vectors for gene therapy or encapsulated drug carriers.

MATERIALS AND METHODS

Dorsal Chamber and Tumor Implantation. Dorsal chambers were implanted in severe combined immunodeficient mice as described in Leunig *et al.* (11). The cell lines studied were LS174T, human colon adenocarcinoma (ATCC); MCa IV, murine mammary carcinoma; HCa-1, murine hepatoma; Shionogi, male testosterone-dependent mammary carcinoma (kindly provided by M. E. Gleaze, Division of Urology, University of British Columbia, Vancouver, Canada), and ST-8 and ST-12, murine fibrosarcoma (kindly provided by L. Gerweck and T. Syed, Radiation Oncology, Massachusetts Gen-

The publication costs of this article were defrayed in part by page charge payment. This article must therefore be hereby marked "*advertisement*" in accordance with 18 U.S.C. §1734 solely to indicate this fact.

This paper was submitted directly (Track II) to the *Proceedings* office.
Abbreviations: VVO, vesicular vacuolar organelles; VEGF, vascular endothelial growth factor; bFGF, basic fibroblast growth factor; Rho-BSA, tetramethylrhodamine-labeled BSA.
‡S.K.H. and W.L.M. contributed equally to this work.
¶Present address: Department of Biomedical Engineering, Box 90281, Duke University, Durham, NC 27708.
††To whom reprint requests should be addressed. e-mail: Jain@steele.mgh.harvard.edu.

eral Hospital, Boston). Cultured cells were dispersed with trypsin/EDTA and transferred into DMEM. Two microliters of dense suspension (containing ≈2 × 105 cells) LS174T was inoculated onto the striated muscle layer of the subcutaneous tissue in the chambers. For the implantation of MCa IV, HCa-1, Shiniogi, ST-8, and ST-12 a piece of tumor tissue, 1 mm in diameter (or 0.5 μl), was placed onto the striated muscle. The experiments were performed between 14 and 20 days after tumor implantation, depending on the growth and vascularization of the tumor. Tumor size was within 30–50% of chamber window size at the time of studies (4–6 mm in diameter).

Cranial Window and Tumor Implantation. Cranial windows were implanted into severe combined immunodeficient mice as described in Yuan *et al.* (12). The cell lines studied were MCa IV, HCa-1, Shionogi, ST-8, and U87 (human glioblastoma; ATCC, Rockville, MD). Experiments were performed 7 days after implantation in the cranial window for all tumors except U87. U87 required a 14- to 20-day growth period before significant vasculature appeared. The tumors were 3–5 mm in diameter and well vascularized.

bFGF-Impregnated Collagen Gel Implantation. Collagen gels were implanted into dorsal chambers by using the procedure described previously by Dellian *et al.* (13). Human recombinant bFGF (GIBCO/BRL) was suspended in aluminum sucrose octasulfate (sucralfate; courtesy of Bukh Meditec, Copenhagen, Denmark), and collagen type I (Vitrogen 100, Celtrix Laboratories, Palo Alto, CA) in the following ratios: 600 ng of bFGF dissolved in 24 μl of 0.1% BSA (Sigma), 176 μl of collagen, plus 6.5 mg of sucralfate. The implanted device consisted of two polymer meshes sandwiching the collagen gel.

Hormone Ablation. Animals implanted with Shionogi tumors in the dorsal chamber were divided into two groups after 10 to 12 days of tumor growth. Half of the animals were orchiectomized, the other half underwent sham operations. At the time of orchiectomy the tumors were 5–7 mm in diameter and well vascularized. The pore cutoff size was determined, as described below, at 2 days before, the day of, 2 days after, and 4 days after either orchiectomy or sham surgery.

Long-Circulating Liposome and Latex Microsphere Preparation. Long-circulating polyethylene glycol-coated rhodamine-labeled liposomes or latex microspheres were prepared as described by Yuan *et al.* (12). Particle size was determined by using a Coulter N4 MD Particle Size Analyzer.

Experimental Procedure. Animals bearing dorsal chambers or cranial windows were anesthetized with a subcutaneous injection of a mixture of 90 mg of Ketamine (Parke–Davis) and 9 mg of Xylazine (Fermenta, Kansas City, MO) per kg of body weight. A 200-μl suspension of long-circulating liposomes ranging in size from 100 to 580 nm or latex beads sized at 780 nm, 1.2 μm, and 2 μm were injected into the tail vein of the mouse (n = 4 mice for each size). The extent of particle extravasation was observed 24 hr after injection, to allow for clearance from the circulation and for better resolution. However, particles were noted to extravasate from vessels within 1 min of i.v. injection. Microvascular extravasation was observed by using a ×20 long-working distance objective and an intravital fluorescence microscope (Axioplan, Zeiss) using transillumination and epiillumination (model 770; OptiQuip, Highland Mills, NY) with fluorescence filters for FITC (excitation, 450–490 nm; emission 515–545 nm) or Rhodamine (excitation, 525–550 nm; emission 580–635 nm) (Omega Optical, Brattleboro, VT). Images of the tumors were acquired with a 35-mm camera (HFX-DX; Nikon) using 1,000 ASA 35-mm film (Kodak).

The entire area of the tumor was scanned for extravasation of rhodamine labeled long-circulating liposomes or latex microspheres. The criterion for extravasation was the presence of fluorescence in the interstitial space in five or more fields of vision over the tumor, 24 hr after injection. Normal tissue surrounding the tumor implant was also examined for extravasation. The pore cutoff size was determined as the range between the largest particle size that could extravasate and the smallest size that could not extravasate, as described previously (4). Vascular density was qualitatively assessed, and all tumors were judged to be well vascularized at the time of these studies.

Electron Microscopy. Tumors (less than 5-mm thick × 8 mm in diameter) were removed from dorsal chambers and submerged in 1.5% glutaraldehyde in 0.1 M sodium cacodylate-HCL (pH 7.4) with 5% sucrose for 1–3 hr. Tumors were then trimmed to 1-mm^3 pieces and processed for electron microscopy as previously described (8). Briefly, after three washes in cacodylate buffer with 7.5% sucrose, trimmed tumor pieces were postfixed in cacodylate buffered (pH 7.4), 1% OsO_4 on ice for 1 hr, stained with uranyl acetate overnight, dehydrated, embedded in EPON 812, and cured for 24 hr at 60°C. Thin (50-μm) sections were cut, stained with uranyl acetate and lead citrate, examined, and photographed on a Phillips CM10 electron microscope at 80–100 kV. Morphometric analysis on open endothelial gaps and endothelial fenestrations was completed on 100-nm long-circulating liposome-injected and noninjected mice. Data were compiled from 3 tumors (6–9 samples from the same tumor type) from noninjected mice and 7 tumors (14 blocks) from liposome-injected mice.

Permeability Measurements. The experimental procedure was described previously (14). Briefly, anesthetized animals were injected i.v. with 0.15 ml of tetramethylrhodamine-labeled BSA (Rho-BSA; Molecular Probes), and intravital fluorescence microscopy (Axioplan, Zeiss) with a fluorescence filter for rhodamine (excitation, 525–550 nm; emission 580–635 nm), intensified charge-coupled device video camera (C2400-88, Hamamatsu Photonics, Hamamatsu City, Japan), and photomultiplier (9203B; EMI, Rockaway, NJ) was performed. An image of the vasculature was recorded on videotape for off-line analysis of vessel diameter and length, and the background intensity was measured under epifluorescence illumination (100-W mercury lamp, model 770; OptiQuip). A bolus injection of Rho-BSA was given via the tail vein (0.15 ml over 20 sec). The fluorescence intensity was measured at 2-min intervals for 20 min; the time interval for each observation was 10 sec (14).

RESULTS

Tumor Microvessels Have a Characteristic Pore Cutoff Size. The first goal of this study was to characterize the pore cutoff size, a functional description of the size of the transvascular gaps based on the size at which the particle extravasates and the upper limit of the particle size at which no extravasation occurs. Five murine tumors (HCa-I, MCa IV, Shiniogi, ST-8, and ST-12) and one human tumor (LS174T) implanted in the dorsal skin-fold chamber were studied. For example, 380-nm long-circulating liposomes extravasated from the vessels of HCa-I tumors implanted in the dorsal chamber, whereas 550-nm long-circulating liposomes did not extravasate (Fig. 1, HCa-I). The majority of tumors exhibited a vascular pore cutoff size between 380 and 780 nm (Fig. 1). A notable exception to this was the MCa IV, which exhibited a cutoff size between 1.2 and 2 μm. All vessels with perivascular accumulation of extravasated particles were well perfused in all the tumors studied. There was no extravasation of any long-circulating liposomes or latex microspheres from microvessels in the normal tissue surrounding the tumor in the dorsal skin-fold chamber.

Electron microscopy of MCa IV microvasculature supports these functional observations. From a total of 142 tumor vessels analyzed from mice that did not receive long-circulating liposome i.v. injections, 56 (39.4%) had fenestrated endothelium and 15 (10.6%) had open endothelial gaps. These results were not significantly different from those obtained from

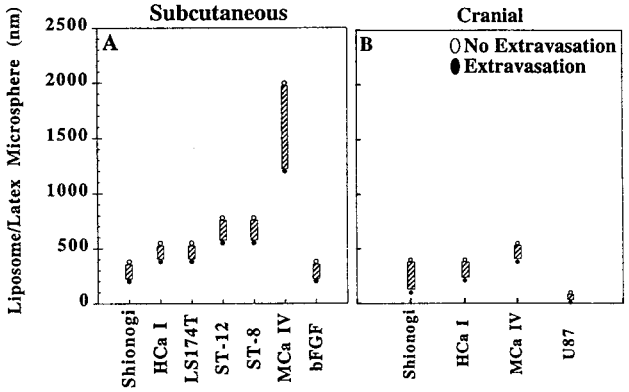

FIG. 1. The vascular pore cutoff size for six different types of tumors grown in the dorsal chamber (*A*) and four tumors grown in the cranial window (*B*) was evaluated. The solid circles represent significant extravasation at the indicated long-circulating liposome or latex bead size. The open circles represent no extravasation at the indicated liposome/latex bead size. The size range between the last particle extravasated and the first particle that did not extravasate indicates the vascular pore cutoff size range (hatched bar). The majority of tumors have a vascular pore cutoff size range between 380 and 780 nm when grown subcutaneously in the dorsal chamber. The interaction of the tumor with the cranial microenvironment (*B*) leads to a smaller vascular pore cutoff size than the interaction of the same tumor with the subcutaneous microenvironment (*A*). Comparison of bFGF-induced vessels (bFGF) and tumor-induced vascular pore sizes demonstrates that the presence of bFGF alone can lead to pores of this size.

animals that were injected with long-circulating liposomes [442 tumor vessels; 124 with fenestrated endothelium (28.1%); 40 with open gaps (9.1%)] (Table 1). The mean number of fenestrations per vessel profile in tumor vessels that had fenestrated endothelium was 8 ± 0.8 for noninjected animals and 5 ± 0.4 for injected animals. Fenestrated endothelium was observed in capillary-sized and venular-sized vessels (Fig. 2*A*). Open endothelial gaps ranged in size from 100 to 1,000 nm, although the majority of the gaps were between 200 and 900 nm (Fig. 2*B*). Without serial sections and reconstruction we could not determine whether these open endothelial gaps were interendothelial or transendothelial. Long-circulating liposomes (100 nm) were also seen extravasating through open junctions (Fig. 2*C*).

The Host Microenvironment Modulates Tumor Microvascular Pore Cutoff Size. To determine the effect of the cranial microenvironment on pore cutoff size, similar studies were performed on tumors grown in the cranial window. The tumors generally grew twice as fast in this location as they did when grown subcutaneously (data not shown). The vascular pore cutoff size was dramatically smaller in all tumors when grown in the pial microenvironment of the cranial window as compared with the same tumor grown in the subcutaneous microenvironment of the dorsal chamber (Fig. 1 and Table 2). The adjacent normal pial tissue did not exhibit extravasation of any long-circulating liposome or latex microspheres. The vessels were well perfused throughout the tumors.

Hormone Withdrawal Decreases Pore Cutoff Size in Hormone-Dependent Tumors. The hormonal milieu as a specific component of the microenvironment has been shown to regulate angiogenesis in hormone-dependent mammary carcinomas (15). To demonstrate a role for steroid hormones in the maintenance and modulation of the pore cutoff size,

Table 1. MCa IV vessel morphometry by electron microscopy

Tracer	Vessels counted	% fenestrated	% open junctions
No liposomes	142	39.4	10.6
Liposomes	442	28.1	9.1

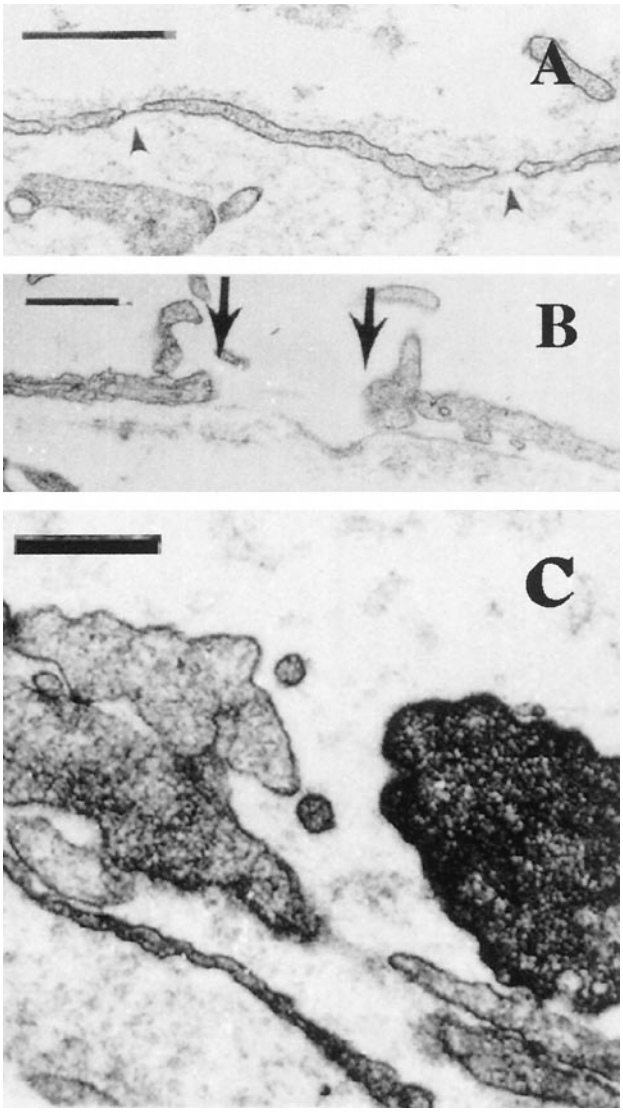

FIG. 2. Representative electron micrographs of MCa IV tumor vessels grown in the dorsal chamber. (*A*) Venular-sized vessel with fenestrated endothelium (arrowheads). (Bar = 500 nm.) (*B*) Tumor vessel with an open gap measuring 856 nm delineated by the arrows. (Bar = 500 nm.) (*C*) Open endothelial gap in tumor blood vessel from a long-circulating liposome-injected animal. What appear to be long-circulating liposomes are shown traversing through the open junction. Serial sections (not shown) demonstrate that these are not transverse sections of cellular projections. (Bar = 300 nm.)

microvascular growth and regression were followed for 27 days in Shionogi (testosterone-dependent) tumors before and after hormone ablation. Initial vascularization was vigorous and occurred within 7 days. Before 7 days the vasculature was composed of very thin tortuous vessels, in agreement with previous studies of the changing microvasculature in LS174T tumors (11). Orchiectomy or sham surgery was performed on days 10–12, determined by the rate of vascularization of the tumors in a given cohort. Vascular regression occurred with hormonal withdrawal whereas continued tumor growth oc-

Table 2. Pore cutoff size: Dorsal chamber vs. cranial window

Tumor cell line (n = 5)	Dorsal chamber pore cutoff size, nm	Cranial window pore cutoff size, nm
HCa-I	380–550	210–380
Shionogi	200–380	100–380
MCa IV	1,200–2,000	380–550

curred in the sham-operated mice (Fig. 3). Pore cutoff size measurements were made 2 days before surgery, the day of surgery, and 2 and 4 days after surgery (different cohorts of animals were used for each time point and particle size; n = 5 sham operated and n = 5 orchiectomized animals for each long-circulating liposome size, as well as for albumin) (Fig. 4). The continuous rearrangement of the blood vessels during tumor growth (Fig. 3) did not lead to any change in the vascular pore size (Fig. 4*A*). A rapid and significant decrease in vascular pore cutoff size was observed 48 hr after orchiectomy (Fig. 4*B*). Fluorescein isothiocyanate-BSA (≈7 nm) extravasates in orchiectomized animals after 48 hr.

bFGF-Induced Vessels Have a Pore Cutoff Size Similar to That Seen in Tumors. Angiogenic vessels were induced in a bFGF (3,000 ng/ml) containing collagen/sucralfate gel, implanted in a dorsal chamber (13). We found that the vascular pore size range of vessels in these gels was 200–380 nm (Fig. 1, bFGF). Inflammation because of irritation by the nylon mesh may be responsible for vessels growing into the side of the gels. No liposomes extravasated from these vessels or from vessels in normal tissue surrounding the gel.

Effective Microvascular Permeability Is Independent of Pore Cutoff Size. The effective microvascular permeability to Rho-BSA was measured in HCa-I, MCa IV, and ST-8 tumors transplanted in dorsal chambers (Table 3). These tumors spanned the entire range of vascular pore cutoff sizes (Fig. 1). The permeability of LS174T has been determined in a previous study (16). All tumors were hyperpermeable to Rho-BSA relative to normal tissue. The permeabilities were not statistically different from each other (ANOVA), even though the pore cutoff sizes were quite different (Table 3).

DISCUSSION

Pore Cutoff Size Determination. In this study we report the pore cutoff size, as defined by Yuan *et al.* (16), for various tumors. Tumors are shown to have a characteristic pore cutoff size, the majority ranging between 380 and 780 nm. It appeared that smaller, 100- to 200-nm long-circulating liposomes extravasated more diffusely along the vessel whereas larger, 380- to 780-nm particles extravasated in a more focal manner, suggesting a heterogeneity in pore sizes along the vessel, although this also may have been because of the smaller-sized particles diffusing further through the interstitium. Spatial heterogeneity in the distribution of fenestrations and open endothelial gaps in tumor vessels have been noted by Roberts and Palade (8).

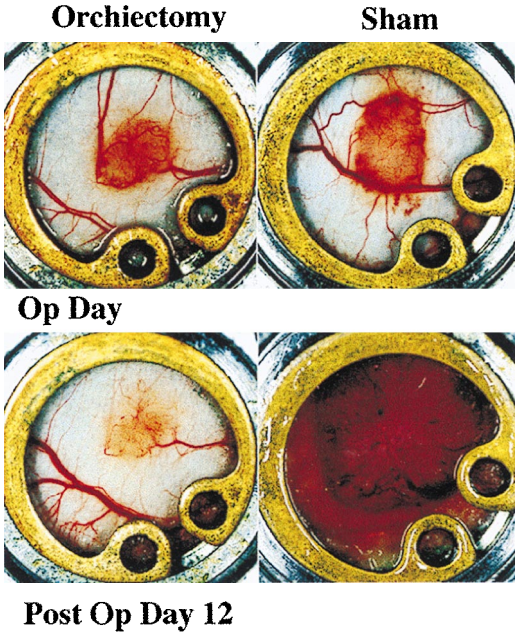

FIG. 3. Comparison of the tumor size and vascularization during growth and regression of Shionogi xenografts in the dorsal chamber. Orchiectomy or sham operation was conducted after 11 days of tumor growth (Op Day). Tumor regression and growth is documented at postoperative day 12 for orchiectomized and sham-operated mice, respectively.

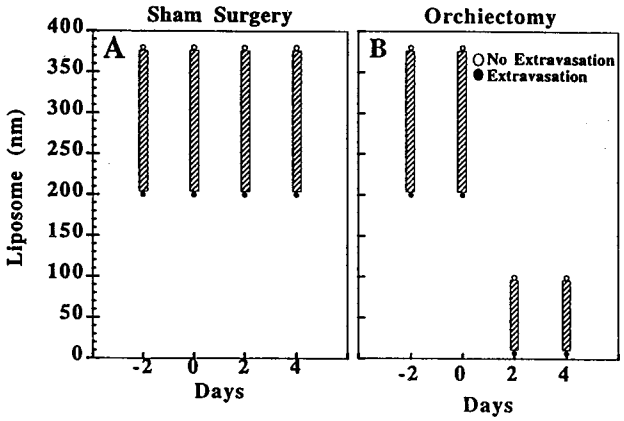

FIG. 4. Shionogi tumors were implanted in the dorsal chamber of male severe combined immunodeficient mice, and pore cutoff size was determined during microvascular growth and regression for a maximum of 27 days. Initial vascularization occurred within 7 days. Day 0 corresponds to the date of orchiectomy or sham operation, day −2 is 48 hr before the surgery, and day 2 is 48 hr after surgery. (*A*) Sham-operated. Once the tumors were vascularized, there was no change in the vascular pore cutoff size with further growth of the tumor. (*B*) Orchiectomized. However, there was a rapid and striking decrease in the vascular pore cutoff size with hormone-withdrawal-mediated tumor regression. The vascular pore cutoff size returned to that of normal tissue within 48 hr after orchiectomy.

The hyperpermeable nature of the tumor microcirculation is well documented (3, 11, 14, 17). Numerous morphological studies have demonstrated the existence of interendothelial junctions, transendothelial channels, fenestrations, and VVO in tumor vessels (8, 10, 18). It remains controversial as to which pathways are predominantly responsible for tumor hyperpermeability and macromolecular transvascular transport. Based on the observed size of the extravasated long-circulating liposomes and latex beads it seems that the transvascular transport, observed in this functional study, is due to either interendothelial or transendothelial open junctions. Normal vessels have interendothelial junctions or clefts with an effective size of 6–7 nm (19). Widened interendothelial junctions have been described in tumors (8). It is generally accepted that the caveolae or vesicle diameter is between 50 and 70 nm (18, 20, 21). VVOs are described in tumor microvessels and normal postcapillary venules (18); however, only tumor microvessels are hyperpermeable. On average, the vacuoles involved in

Table 3. Pore cutoff size vs. effective permeability to BSA

Tumor cell line (n)	Pore cutoff size, nm	Permeability ($\times 10^7$ cm/sec)
HCa-I (5)*	380–550	2.06 ± 1.44 (1.60–3.99)
LS174T (6)*†	400–600	1.24 ± 0.45 (0.56–1.67)
ST-8 (5)*	550–780	3.73 ± 3.34 (1.67–9.28)
MCa IV (8)*	1,200–2,000	2.5 ± 1.5 (1.2–5.1)
MCa IV (6)§	380–550	1.9 ± 0.5 (1.3–2.5)
U87 (6)‡	7–100	3.8 ± 1.2 (2.4–5.0)

n, number of animals.
*Grown in dorsal chamber.
†Yuan *et al.* (16).
‡Grown in cranial window.
§Yuan *et al.* (12).

VVOs are larger than caveolae size (108 ± 32 nm inner diameter) (22). Tumor vessels have been shown to have fenestrations that are approximately 60 nm (8), whereas endothelial cells in the liver sinusoids contain large fenestrations (without diaphragms) approximately 106–175 nm in diameter (23). Pulmonary endothelial cells have been shown to phagocytose 5- to 10-μm beads (24); however, this mechanism has not been described in tumor vessels.

Electron microscopy of the MCa IV microvasculature supports these functional studies. In agreement with previous reports (8), fenestrated endothelium were observed consistently in every tumor sample, although less frequent, open endothelial gaps were also observed. It was not possible to determine whether these open endothelial gaps were interendothelial or transendothelial without serial sections and three-dimensional reconstruction (10). Despite years of carefully controlled studies to the contrary (25, 26) it has recently been reported that open endothelial gaps are an artifact from colloidal tracer injection (22). Experiments thus were designed to specifically address whether the tumor vascular endothelial morphology was adversely affected by the injection of long-circulating liposomes or latex beads. These results demonstrate that there is no statistical difference between injected and noninjected animals with respect to the percentage of fenestrated vessels or open endothelial gaps. In micrographs, endothelial gaps ranged from 100 to 1,000 nm, but the majority were approximately 700 nm. The discrepancy between functional (intravital microscopy) and structural (electron microscopy) gap size of the MCa IV tumor is likely because of differences in sample size and methodologies. Although sufficient samples were observed to provide statistically meaningful data, the number of vessels observed with intravital microscopy is much greater than with electron microscopy. Furthermore, the gaps observed with intravital microscopy are pliable and can dynamically adjust to larger particles, whereas all gaps observed by electron microscopy are fixed and gap size might have become smaller with fixation.

Microenvironmental Modulation of the Pore Cutoff Size. The interactions between the tumor and the host microenvironment are known to affect tumor physiology and phenotype (27). Vascular permeability has been shown to be modulated by the local microenvironment (5, 12, 13). This study shows that the local host microenvironment plays a role in determining tumor pore cutoff size. The tumor pore cutoff sizes observed in the cranial window were dramatically smaller than those of the same tumors implanted into the dorsal chamber (Fig. 1, Table 2). Molecules within the cerebral microenvironment form and regulate the blood–brain barrier (28), whereas tumor cells produce specific cytokines, growth factors, and enzymes conducive to hyperpermeability (29). It is most likely the balance between host- and tumor-elaborated factors that leads to the observed smaller microvessel pore cutoff size. Similar interactions between host and tumor tissues occur in the dorsal chamber. However, the normal subcutaneous endothelium does not exhibit a tight barrier such as that found in the blood–brain barrier, so these tumor vessels would be expected to have a larger pore cutoff size than when grown in the cranial window. Differential expression of angiogenic growth factors such as bFGF and VEGF, as well as their receptors, and inhibitors has been demonstrated in various tumors (30) and is expected in these different microenvironments. *In situ* hybridization studies of VEGF and its two receptors in human glioma HGL21 grown in cranial windows and subcutaneously did not show significant differences (unpublished data), although permeability and pore cutoff size is lower in tumors grown in the cranial window. This suggests that other factors in the cranial microenvironment may reduce the net pore cutoff size and permeability.

Hormonal Regulation of the Pore Cutoff Size. The hormonal milieu is a specific component of the microenvironment. Here we show that the tumor microvasculature of Shionogi Carcinoma 115 (Shionogi), an androgen-dependent mouse mammary tumor (31), is maintained in the presence of androgen but quickly regresses with hormonal ablation. Furthermore, vessel rarefaction is preceded by a dramatic decrease in the pore cutoff size.

Tumor tissue regression shown here correlated well with other studies (32, 33). We observed vascular regression concomitant with androgen ablation. Whether this is a direct effect of androgen withdrawal on the endothelial cells or an indirect effect resulting from reduced levels of VEGF production by cancer cells remains unclear. Shionogi cells undergo apoptosis with androgen withdrawal (unpublished data). Furthermore, VEGF has been shown to be directly regulated by hormonal levels (34). The treatment of tumors with anti-VEGF antibodies reduced permeability and led to vessel regression in solid tumors (6), which is similar to what we show with hormonal withdrawal. Thus, it appears that hormonal ablation therapy mimics anti-VEGF therapy to some extent. These results, taken together with the work of Yuan *et al.* (6), imply that hormonal ablation and anti-angiogenic therapies (that target VEGF) may decrease the transvascular transport of other therapeutic agents one might want to deliver in combination or subsequently. Thus, strategies such as chemotherapy, immunotherapy, and gene therapy may need to be used before hormone ablation therapies or other therapies that may reduce transvascular transport.

Growth Factor Modulation of Pore Cutoff Size. bFGF is one of the most potent angiogenic factors and serves as an endothelial mitogen, promoting proliferation, migration, and synthesis of plasminogen activators (35, 36). In this study we demonstrated that angiogenic vessels stimulated by bFGF have a pore cut off size of 200–380 nm. This pore cutoff size is significantly higher than normal vessels and is similar to some tumors grown in the dorsal chamber. Previous studies indicate that acute treatment with bFGF does not modify vascular permeability, whereas topical treatment with VEGF does transiently increase vascular permeability (37). However, Elvax pellets containing 0.5–2 μg bFGF that was implanted subcutaneously resulted in the formation of vessels having ($\approx$60 nm) fenestrations and open interendothelial junctions (8). Thus, the results from this study and previous studies indicate that chronic exposure to bFGF could affect the pore cutoff size. Because bFGF is used in various gel assays of angiogenesis and anti-angiogenesis (38), these results are useful.

Effective Permeability Determination. Transvascular transport of albumin ($\approx$7 nm) in the tumor can occur via all the pathways described. In the present study, we found no correlation of the tumor microvessel pore cutoff size with permeability to Rho-BSA. It appears that the transport of Rho-BSA is not hindered because the radius of the transendothelial pathways is much larger than the radius of BSA in the tumors studied.

It is interesting to note that the pore cutoff size of MCa IV is much larger than that of U87 in the cranial window. However, the permeability to BSA in U87 (3.8×10^{-7} cm/sec) is roughly two times higher than that in MCa IV (1.9×10^{-7} cm/sec) in the cranial window. This is because permeability is determined by the total cross-sectional area of transvascular pores, when the pore size is much larger than the size of the particle leaving the vessel. Thus, U87 vessels may have many more frequent but smaller pores than the MCa IV vessels. Although it would be expected that albumin transvascular transport occurs by diffusion through large open gaps, the possibility that albumin is transported by other methods, such as VVOs or receptor-mediated pathways (22, 39), cannot be excluded.

This study demonstrates that tumor vessels have a characteristic pore cutoff size that seems to be maintained by both

local microenvironmental factors and the tumor milieu. In most tumors studied, the pore cutoff size was between 380 and 780 nm. Most long-circulating liposomes and viral vectors, proposed for therapeutic use, are between 100 and 300 nm and would extravasate through the passageways described. However, tumors grown in the cranial microenvironment and hormone-dependent tumors after hormonal ablation have a significantly smaller pore cutoff size. These smaller open gaps may limit transvascular transport of large therapeutic agents. Recently, the use of gene therapies for solid tumors and the limitations of various gene vectors were described (40, 41). These and other therapeutic approaches may also be limited by the transvascular transport of the agent. An understanding of the limits and regulation of transvascular transport may offer modalities to increase the distribution or size of the transvascular transport pathways for optimized delivery of large therapeutic agents.

We thank Drs. Dai Fukumura, Yves Boucher, David Berk, and Lance Munn for reviewing this manuscript and providing many helpful comments, as well as Sylvie Roberge, Julia Khan, and Yi Chen for their outstanding technical assistance. This work was supported by an Outstanding Investigator Grant from the National Cancer Institute (R35-CA56591) awarded to R.K.J. S.K.H. is supported by a National Institutes of Health Medical Research fellowship (F32). W.L.M. is supported by a National Cancer Institute Research Fellowship (T32).

1. Gerlowski, L. & Jain, R. (1986) *Microvasc. Res.* **31,** 288–305.
2. Jain, R. (1996) *Science* **271,** 1079–1080.
3. Jain, R. (1987) *Cancer Metastasis Rev.* **6,** 559–593.
4. Yuan, F., Dellian, M., Fukumura, D., Leunig, M., Berk, D., Torchillin, V. & Jain, R. (1995) *Cancer Res.* **55,** 3752–3756.
5. Fukumura, D., Yuan, F., Monsky, W., Chen, Y. & Jain, R. (1997) *Am. J. Pathol.* **151,** 679–688.
6. Yuan, F., Chen, Y., Dellian, M., Safabakhsh, N., Ferrara, N. & Jain, R. (1996) *Proc. Natl. Acad. Sci. USA* **93,** 14765–14770.
7. Dvorak, H., Brown, L., detmar, M. & Dvorak, A. (1995) *Am. J. Pathol.* **146,** 1029–1039.
8. Roberts, W. & Palade, G. (1997) *Cancer Res.* **57,** 765–772.
9. Baluk, P., Hirata, A., Thurston, G., Fujiwara, T., Neal, C., Michel, C. & McDonald, D. (1997) *Am. J. Physiol.* **272,** L155–L170.
10. Neal, C. & Michel, C. (1995) *J. Physiol.* **488,** 427–437.
11. Leunig, M., Yuan, F., Menger, M., Boucher, Y., Goetz, A., Messmer, K. & Jain, R. (1992) *Cancer Res.* **52,** 6553–6560.
12. Yuan, F., Salehi, H., Boucher, Y., Vasthare, U., Tuma, R. & Jain, R. (1994) *Cancer Res.* **54,** 4564–4568.
13. Dellian, M., Witwer, B., Salehi, H., Yuan, F. & Jain, R. (1996) *Am. J. Pathol.* **149,** 59–71.
14. Yuan, F., Leunig, M., Berk, D. & Jain, R. (1993) *Microvasc. Res.* **45,** 269–289.
15. Gagliardi, A. & Collins, D. (1993) *Cancer Res.* **53,** 533–535.
16. Yuan, F., Leunig, M., Huang, S., Berk, D., Papahadjoupolos, D. & Jain, R. (1994) *Cancer Res.* **54,** 3352–3356.
17. Dvorak, H., Nagy, J., Dvorak, J. & Dvorak, A. (1988) *Am. J. Pathol.* **133,** 95–109.
18. Kohn, S., Nagy, J., Dvorak, H. & Dvorak, A. (1992) *Lab. Invest.* **67,** 596–607.
19. Lum, H. & Malik, A. (1994) *Am. J. Physiol.* **267,** L223–L241.
20. Michel, C. (1992) *Am. Rev. Respir. Dis.* **146,** s32–s36.
21. Palade, G. & Milici, A. (1991) *Mol. Mechanisms Cell Growth Differ.* **2,** 223–247.
22. Feng, D., Nagy, J., Hipp, J., Dvorak, H. & Dvorak, A. (1996) *J. Exp. Med.* **183,** 1981–1986.
23. Ballet, F. (1990) *Pharm. Ther.* **47,** 281–328.
24. Ryan, U. (1986) *Fed. Proc.* **45,** 101–108.
25. Majno, G., Palade, G. & Schoefl, G. (1961) *J. Biophys. Biochem. Cytol.* **11,** 607–626.
26. Baluk, P. & McDonald, D. (1994) *Am. J. Physiol.* **266,** L461–L468.
27. Kerbel, R. (1995) *Cancer Metastasis Rev.* **14,** 259–262.
28. Risau, W. (1991) *Ann. N. Y. Acad. Sci.* **633,** 405–419.
29. Senger, D., Brown, L., Claffey, K. & Dvorak, H. (1994) *Invasion Metastasis* **14,** 385–394.
30. Folkman, J. (1995) *Nat. Med.* **1,** 27–31.
31. Minesita, T. & Yamaguchi, K. (1964) *Steroids* **4,** 815–830.
32. Koga, M., Kasayama, S., Matsumoto, K. & Sato, B. (1995) *J. Steroid Biochem. Mol. Biol.* **54,** 1–6.
33. Furuya, Y., Isaacs, J. & Shimazaki, J. (1995) *Jpn. J. Cancer Res.* **86,** 1159–1165.
34. Shweiki, D., Itin, A., Gitay-Goren, H., Neufeld, G. & Keshet, E. (1993) *J. Clin. Invest.* **91,** 2235–2243.
35. Norrby, K. (1994) *Microvasc. Res.* **48,** 96–113.
36. Tabata, Y., Hijikata, S. & Ikada, Y. (1994) *J. Controlled Release* **31,** 189–199.
37. Roberts, W. & Palade, G. (1995) *J. Cell Sci.* **108,** 2369–2379.
38. Jain, R., Schlenger, K., Hockel, M. & Yuan, F. (1997) *Nat. Med.* **3,** 1203–1208.
39. Schnitzer, J. & Oh, P. (1994) *J. Biol. Chem.* **269,** 6072–6082.
40. Verma, I. M. & Somia, N. (1997) *Nature (London)* **389,** 239–242.
41. Blaese, R. (1997) *Sci. Am.* **276,** 111–115.